# Burst Capacity and Spoolability Analysis of Reinforced Thermoplastic Pipes used in the Offshore Oil and Gas Industry

*Alex M. Goddard*[1]

*University of New South Wales at the Australian Defence Force Academy*

**The increasing use of Reinforced Thermoplastic Pipes in the offshore oil and gas industry has led to the necessity to understand how these pipes behave under a range of loading cases. This project aims to analyse the behaviour of Reinforced Thermoplastic Pipes under the effects of internal pressure and under bending. This report presents findings as a result of simulations conducted using these loading cases relating specifically to when failure occurs. The analyses undertaken provide insight into means to predict the maximum internal pressure and the minimum bend radius a specific Reinforced Thermoplastic Pipe can be exposed to.**

## Contents



## Nomenclature

$E =$ Modulus of Elasticity
$E_1 =$ Modulus of Elasticity in the fibre direction
$E_2 =$ Modulus of Elasticity in transverse direction
$E_f =$ Modulus of Elasticity of the fibre material
$E_m =$ Modulus of Elasticity of the matrix material
$\nu =$ Poisson's Ratio
$\nu_{12} =$ Major Poisson's Ratio
$\nu_{21} =$ Minor Poisson's Ratio
$\nu_f =$ Poisson's Ratio of the fibre material
$\nu_m =$ Poisson's Ratio of the matrix material
$G_{12} =$ Shear modulus
$G_m =$ Shear modulus of the matrix material

[1] SBLT, RAN, School of Engineering & Information Technology. ZEIT4501.

$\varepsilon_x$ = Generalized strain in the x direction

$\varepsilon_y$ = Generalized stain in the y direction

$N_x$ = Stress resultant in the x direction

$N_y$ = Stress resultant in the y direction

$B_{ij}$ = Membrane stiffness coefficient

$A_{ij}$ = Stiffness coefficient

$\varepsilon_1$ = Strain in the fibre direction

$\varepsilon_2$ = Strain in the transverse direction

$\gamma_{12}$ = Shear strain

$\sigma_1$ = Stress in the Fibre direction

$\sigma_2$ = Stress in the Transverse direction

$\tau_{12}$ = Shear Stress

$\phi$ = Angle of reinforcement wind

$R$ = Inner Radius

$t$ = Wall Thickness

$P$ = Internal Pressure

# I. Introduction

The use of Reinforced Thermoplastic Pipes (RTP) in the offshore oil and gas industry has become increasingly popular over the past 15 years, and there are indications that this trend will continue (Osborne 2013). This increase in popularity can be attributed to the significant advantages that RTP provide over conventional steel piping; these advantages include an extremely light weight yet high strength pipe, a more sustainable solution due to the corrosion resistance of the RTP and the fact that the installation of RTP is much easier and quicker than that on the conventional steel piping (Dalmolen, Kruyer & Cloos, 2009).

This report aims to identify the burst capacity for a number of different sized RTP to primarily predict the maximum internal pressure of the pipes. Secondly, a Spoolability analysis of the RTP will be undertaken in order to predict the failure mode of the pipe when exposed to a bending load.

## A. Reinforced Thermoplastic Pipe

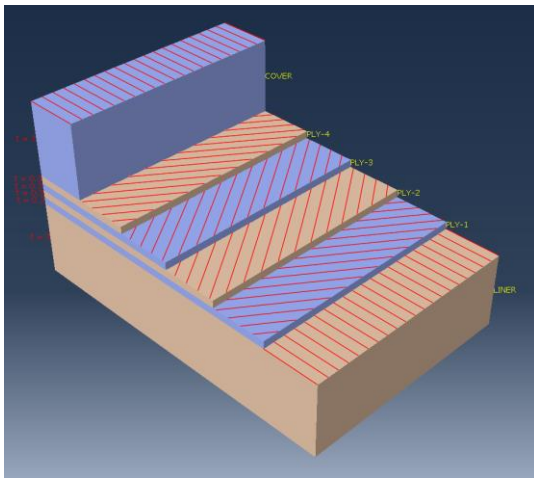


**Figure 1: Ply Stack Plot of RTP**

### *1. Reinforced Thermoplastic Pipe Configuration*

According to the American Petroleum Institute (2006), an RTP is constructed of a number of different layers. These layers consist of a Thermoplastic liner, a number of structural layers and a Thermoplastic Cover. (Conley, Weller & Slingerland, 2008) The Thermoplastic liner is primarily used to provide a leak free and corrosion resistant pipe for the fluid being transported. There is typically an even number of helically wound layers forming the structural layer with the major function to provide the load bearing capacity of the pipe. Finally, the cover is in place to protect the fibres from damage. (Kruijer, Warnet & Akkerman, 2005)

The structural layers are comprised of fibre reinforced thermoplastic lamina, which are wound at an angle of $[\pm 54.7°]_n$, where n is the number of angle-ply layers. It has been proven by use of the netting analysis that this particular wind angle is in fact the optimal wind angle; what this means is that using this wind angle, all stresses produced are in fact in the fibre direction. (Shultz & Smith, 2004)

**Table 2: Properties of PE 80 and Twaron Fibre**

| Mechanical Properties | **PE 80** | **Twaron Fibre** |
|---|---|---|
| **E (MPa)** | 953 | 80000 |
| $\nu$ | 0.42 | 0.38 |

In the analysis' undertaken in this report, the selected materials are Polyethylene 80 (PE80) and Twaron fibre reinforced PE80 angle plies. The total pipe wall thickness is 7mm, with the distribution being 3mm each for the thickness of the liner and cover, and the total thickness of four reinforcement plies being 1.2mm; the ply stack plot can be seen in Figure 1. The material properties of the PE80 and Twaron fibres can be seen in Table 1. In each analysis a number of different inner diameters and lengths have been selected; this is in order to best model what is currently available in industry (Soluforce 2014, Teijin Aramid 2014)

**Table 1: Properties of unidirectional fibre reinforced ply**

| Mechanical Properties | $E_1$ (MPa) | $E_2$ (MPa) | $\nu_{12}$ | $G_{12}$ (MPa) |
|---|---|---|---|---|
| Twaron fibre reinforced PE | 48380 | 953 | 0.396 | 335.6 |

It is important to note that the transverse and shear properties of the ply is dominated by the properties of the matrix material; therefore the transverse and shear moduli of the ply are considered to be equal to that of the PE 80 matrix material. (Yu, et al 2014) As such, the resulting properties of the unidirectional fibre-reinforced ply can be seen in Table 2. The properties of the liner and cover are those of the PE 80. Using the individual material properties of the PE80 and Twaron, the mechanical properties of the unidirectional-fibre reinforced ply can be calculated. These have been calculated using the following equations (Vasiliev & Morozov 2013)

$$E_1 = E_f V_f + E_m V_m \tag{1}$$

$$E_2 = E_m \tag{2}$$

$$\nu_{12} = \nu_f V_f + \nu_m V_m \tag{3}$$

$$\nu_{21} = \frac{E_2 \nu_{12}}{E_1} \tag{4}$$

$$G_{21} = G_m = \frac{E_m}{2(1+\nu_m)} \tag{5}$$

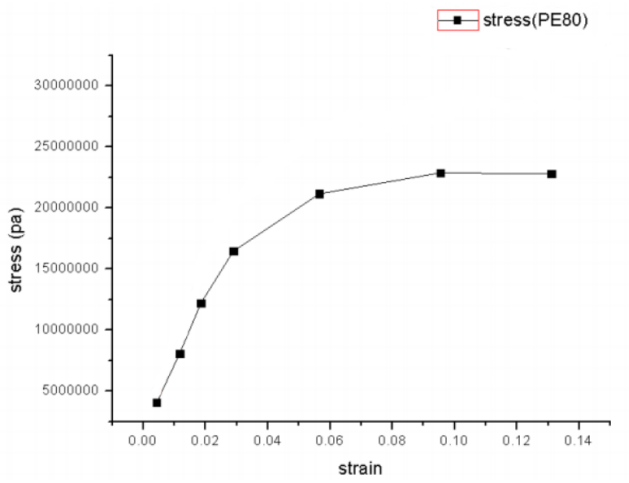


**Figure 2: Stress Strain curve for PE 80**

A major advantage of using PE 80 as the thermoplastic liner, cover and in the reinforcement plies is the way in which it behaves under stress. That is to say because the material is non-linear, once it is under a certain amount of stress, the stress in the material ceases to increase and instead the material begins to strain only. Therefore the material stretches until a fixed amount of strain is reached. The stress strain curve for PE 80 can be seen in Figure 2. This material non-linearity has not been considered fully in this report.

Allowing for the fact that once the stress reaches the limit and it begins to stretch, failure of the pipe is considered to have occurred if the fibres fail in tension or compression, i.e. $\sigma_1 > S_1$. Secondly, if the matrix fails in tension or compression, i.e. $\sigma_2 > S_2$ or if the strain in the liner cover exceed 5.5% failure also is considered to have occurred. The material strengths shall be discussed later.

*2. Reinforced Thermoplastic Pipe Installation*

The installation technique of RTP is called the reel lay. This installation technique involves the unreeling of RTP and then lowering the pipe into the ocean via means of sinking the pipe. When compared with the various methods of installation of conventional steel piping, installation of RTP is extremely advantageous.

A major advantage over conventional steel piping is the fact that RTP is much more flexible. This means that the pipe can be spooled onto reels for transport to the installation site, and then unreeled to be installed. When compared to the transport and installation of steel pipes, this process is comparatively significantly easier.

Typically, steel pipes are installed in one of a few ways; these are S-Lay, J-Lay and Reeling Lay. Reeling Lay, the method of choice for installing RTP, is applicable to laying steel pipes; however the steel pipes are required to have significant plasticity to undergo and withstand the spooling and unspooling motions.

With both S-Lay and J-Lay, the steel pipes need to be welded together prior to entering the ocean. The major difference between the S-Lay and J-Lay techniques is the orientation of the pipes when this welding occurs. For S-Lay the pipes are close to horizontal, and as the pipe goes into the ocean and eventually to the ocean floor, it forms an S shape. Similarly, the J-Lay technique causes the welding to occur at an angle very close to vertical, and when the pipe enters the ocean and rests on the ocean floor, it forms a J shape. (Bai & Bai 2014)

The Reeling Lay technique is comparatively easier as there are no requirement to weld segments of pipe together, the pipe can be unreeled and installed. This means that the installation process is significantly quicker, easier and cost effective.

The Reeling Lay technique forms the basis of the loading types analysed, as the motion of reeling induced bending upon the RTP, as such in order to not damage the pipe it is critical to find the minimum bend radius the pipe can be exposed to prior to material or buckling failure occurring.

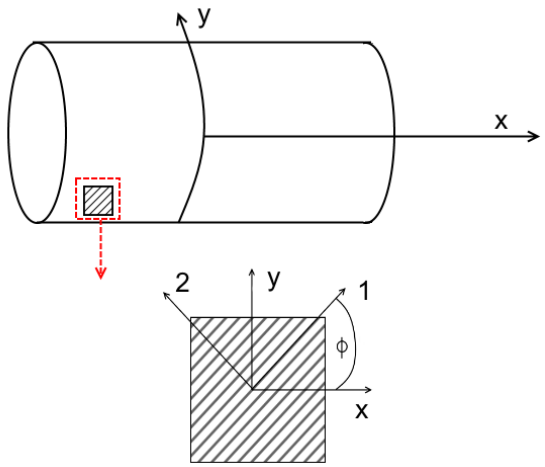


**Figure 3: Global to Local Co-ordinates**

*3. Modelling the RTP Layup in ABAQUS*

In order to successfully model the RTP in ABAQUS, appropriate modelling of the different layers must be done. To model the PE 80 material used as the cover and liner, the *Isotropic* material was selected in the material definition dialog in ABAQUS; in this dialog the elastic modulus and Poisson's ratio of the PE 80 is input. To model the Twaron fibre reinforced ply the Lamina material was selected and the properties listed in Table 1 were input.

To model the different layers on the model, the *Composite Layup* function was used. This function allows the different layers to be applied to the model in the configuration discussed previously. Furthermore, this workbench allows the definition of a specific co-ordinate system to be used, which has been utilised to ensure appropriate stress and strain transformation has occurred in results. The definition of a cylindrical co-ordinate system has been applied and suitably allows for transformation between global x-y co-ordinates to a local 1-2 co-ordinate system.

The use of this local co-ordinate system is important in obtaining correct results from the model after simulations have occurred. Globally, the axial direction has been defined as the x-direction and circumferential direction is the y-direction. For obtaining results from the unidirectional plies, the local co-ordinate system is required, as the stresses and strains that are required are along the fibre and across the fibre also known as the transverse direction. It can be seen in Figure 3 the two co-ordinate systems and how they are related. This cylindrical co-ordinate system was applied to the composite layup to allow the transformation of results from the global to the local co-ordinate systems.

## II. Numerical Analysis

### A. Burst Capacity

The burst capacity of the RTP is modelled as if the RTP is under an internal pressure and has closed ends. This simulation is done in order to predict the maximum internal pressure the pipe can take prior to failure occurring. This modelling is done as predicting the burst capacity of the RTP is an important consideration in the safety and reliability of the RTP in its design and operation. (Bai et al. 2011)

The simulation has been done by modelling the pipe as having a range of different standard diameters, a fixed length of 0.69m and a fixed total wall thickness of 7.2mm. Furthermore, the model has been made out of S4R elements, four node conventional shell elements. (Bai et al, 2011) Failure of the pipe is considered to have occurred when the strain in the liner or cover reaches 5.5% as specified by Chapman, et al (2010) or the stresses in the reinforcement plies exceed the material strength. In the reinforcement plies, the tensile strength in the fibre direction has been found to be 1809 MPa, and because the matrix material dominates the transverse and

shear properties of the reinforcement plies, it has been found experimentally, that the transverse and shear strengths are 22.5MPa and 11.5MPa respectively. (Yu, et al 2014)

In order to predict the results of the full RTP pipe, the process of validating each type of layer occurred. This was done in first modelling the liner and predicting the stresses and comparing to the results obtained via ABAQUS; then validation was undertaken of the structural reinforcement layers. This was done by calculating the stresses in each ply and comparing to results obtained for a pipe modelled as a fully laminated pipe.

Validating the behaviour of the selected model for use in predicting the behaviour of a fully isotropic material pipe was undertaken by creating a composite layup consisting of only an isotropic material. As stated previously, the material was applied as an Isotropic material with the properties of PE 80. The theoretical stresses calculated were the hoop stress and longitudinal stresses. These stresses were then obtained via ABAQUS and compared to the theoretically calculated stresses. It was found that the ABAQUS modelling produced results which correlated to those calculated theoretically; thus it can be seen that the model was valid for an isotropic pipe.

The same process was undertaken in validating the model for its behaviour as a laminated pipe. Similarly, a composite layup was applied and consisted of the four Twaron fibre reinforced layers. The theoretical stresses were calculated using the following series of equations (Vasiliev & Morozov, 2013).

The Stress resultants have been calculated and used to solve for the generalized strains $\varepsilon_x$ & $\varepsilon_y$ using,

$$N_x = PR = B_{11} \cdot \varepsilon_x + B_{12} \cdot \varepsilon_y \tag{6}$$

$$N_y = \frac{PR}{2} = B_{21} \cdot \varepsilon_x + B_{22} \cdot \varepsilon_y$$

The Membrane Stiffness coefficients are found using the following,

$$B_{11} = h \cdot (A_{11}^1 + A_{11}^2 + A_{11}^3 + A_{11}^4) \tag{7}$$

$$B_{22} = h \cdot (A_{22}^1 + A_{22}^2 + A_{22}^3 + A_{22}^4)$$

$$B_{12} = B_{21} = h \cdot (A_{12}^1 + A_{12}^2 + A_{12}^3 + A_{12}^4)$$

where the stiffness coefficients are found using,

$$A_{11}^i = \overline{E_1} \cdot \cos^4 \phi_i + \overline{E_2} \cdot \sin^4 \phi_i + 2 \cdot (\overline{E_1} \cdot \nu_{12} + 2 \cdot G_{12}) \cdot \cos^2 \phi_i \cdot \sin^2 \phi_i \tag{8}$$

$$A_{22}^i = \overline{E_1} \cdot \sin^4 \phi_i + \overline{E_2} \cdot \cos^4 \phi_i + 2 \cdot (\overline{E_1} \cdot \nu_{12} + 2 \cdot G_{12}) \cdot \cos^2 \phi_i \cdot \sin^2 \phi_i$$

$$A_{12}^i = A_{21}^i = \overline{E_1} \cdot \nu_{12} + (\overline{E_1} + \overline{E_2} - \overline{E_1} \cdot \nu_{12} - 2 \cdot G_{12}) \cdot \cos^2 \phi_i \cdot \sin^2 \phi_i$$

where $\overline{E_1} = \frac{E_1}{1 - \nu_{21}\nu_{12}}$ and $\overline{E_2} = \frac{E_2}{1 - \nu_{21}\nu_{12}}$

Finally, using the generalized strains, the strains in the ply can be found,

$$\varepsilon_1^i = \varepsilon_x \cdot \cos^2 \phi_i + \varepsilon_y \cdot \sin^2 \phi_i \tag{9}$$

$$\varepsilon_2^i = \varepsilon_x \cdot \sin^2 \phi_i + \varepsilon_y \cdot \cos^2 \phi_i$$

$$\gamma_{12}^i = 2 \cdot (\varepsilon_y - \varepsilon_x) \cdot \cos \phi_i \cdot \sin \phi_i$$

Which finally allows for the stresses in the fibre and transverse directions and shear stress to be found,

$$\sigma_1^i = \overline{E_1} \cdot (\varepsilon_1^i + \nu_{12} \cdot \varepsilon_2^i) \tag{10}$$

$$\sigma_2^i = \overline{E_2} \cdot (\varepsilon_2^i + \nu_{21} \cdot \varepsilon_1^i)$$

$$\tau_{12}^i = G_{12} \cdot \gamma_{12}^i$$

The stresses obtained via ABAQUS and the stresses calculated through the previous equations provided results that correlated.

Throughout all simulations to find the burst capacity, the boundary conditions and loadings have remained the same. A fixed end boundary condition was applied to one end of the pipe and at the free end there was a boundary condition restricting the movement in all directions except axially. Furthermore, all nodes at the free end have been kinematically coupled to a reference point on the pipes axis and a concentrated force was applied; this force is to simulate a closed end. An internal pressure was applied to the inner face of the model. In order to obtain the stresses in the fibre direction, a cylindrical co-ordinate system was applied to the composite layup; this was discussed previously.

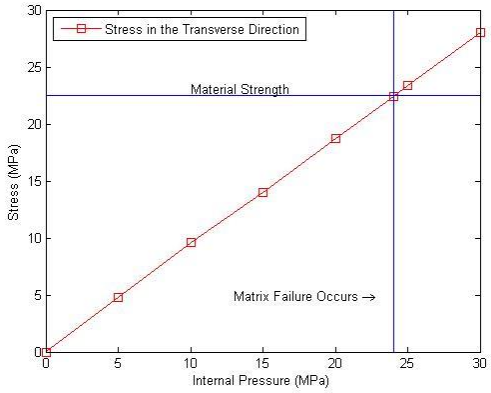


**Figure 4: Stress in the Transverse Direction in Ply-1 resulting from the applied Internal Pressure**

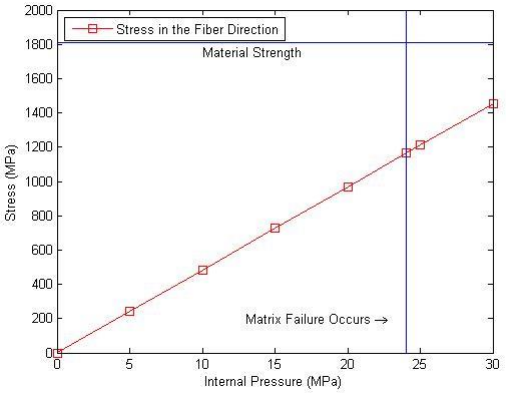


**Figure 5: Stress in the Fibre Direction in Ply-1 resulting from the applied Internal Pressure**

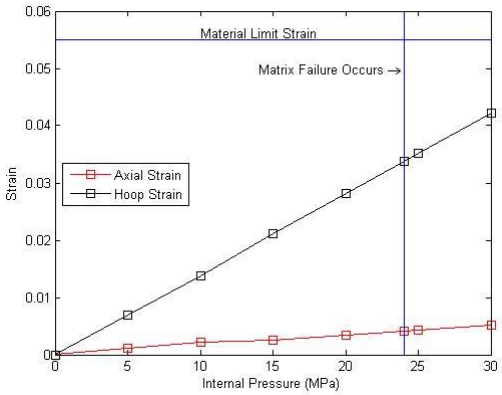


**Figure 6: Strains in the Liner and Cover resulting from the applied Internal Pressure**

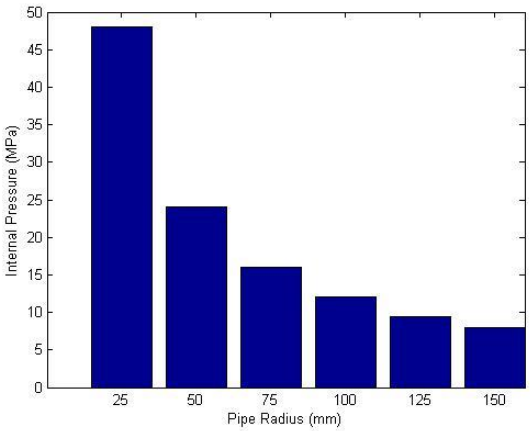


**Figure 7: Burst capacity for various pipe Radius**

To successfully find the burst capacity of the pipe, it was assumed that failure occurred when matrix failure occurred; that is to say that the stress in the transverse direction in the plies is greater than the material strength. In addition to this, if the strain in the liner or cover exceeded the maximum 5.5% then failure was also considered to have occurred.

Consider a full RTP model with radius of 50mm, length of 0.69m, and total wall thickness of 7.2mm. The simulation was run for a number of pressures until one of the failure modes occurred. Figures 4, 5 and 6 denote the results obtained for the simulation.

As it can be seen in Figure 4, when the internal pressure reaches 24MPa, the stress in the transverse direction exceeds the material strength. Figure 5 shows the stress in the fibre direction which when failure occurs is well below the material strength. Figure 6 shows the strains in the liner and cover which are also well below the material strain strength.

What can be taken away from these results is that at the point of transverse failure in the first ply, the stresses and strains in the fibre direction and in the liner and cover are well below their respective material limits. Furthermore, this suggests that failure due to internal pressure is wholly caused by transverse failure of the matrix material.

This same simulation was repeated for a number of different radius models, keeping all parameters fixed. The results obtained via these analyses suggest the same results; that the failure due to internal pressure is in fact due to transverse failure of the matrix material in the reinforcement plies. Furthermore, it can be seen in Figure 7 a plot showing the different radius of RTP models and the internal pressure at which failure occurred.

As it can be seen in Figure 7, for a smaller radius pipe, the internal pressure required to cause the pipe to burst is significantly higher than that required for a pipe of larger diameter.

**B. Spoolability Analysis**

The Spoolability analysis of the RTP is modelled as if the RTP is being spooled onto a reel, simulating the mechanism of storing the RTP. This modelling is done to predict the minimum bend radius that the pipe can be put into before buckling occurs. When compared to conventional steel pipes which undergo plastic deformation when spooled onto a reel, the RTP should be able to flex and be spooled onto much smaller reels; providing a significant advantage over the steel pipes.

The simulations have been undertaken again by modelling different standard sized diameters, two different lengths and a fixed total wall thickness of 7.2mm. The model has been made out of S8R elements, two dimensional eight noded quadrilateral shell elements with six degrees of freedom per node; there are 20 elements circumferentially and 40 along the length of the model. (Ashraf, Morozov & Shankar 2012) Two modes of failure of the pipe have been considered and these are if buckling has occurred or material failure has occurred.

In order to simulate the buckling, one end of the model has been fixed and a rotational displacement has been applied in one direction to the free end. This rotational displacement is applied to a reference point at the free end along the central axis; to ensure that the rotation is applied to all nodes, the reference point is kinematically coupled to all nodes of the cross section.

In all simulations to predict the buckling of the RTP, the boundary conditions and displacements have remained constant. A fixed end boundary condition was applied to the base of the RTP, and a rotational displacement was applied to the free end; this was to simulate the movement associated with reeling. The use of ABAQUS' *History Output* function was used to obtain the reaction moment and rotational displacement over the course of the simulation.

As documented by Brazier (1927), the ovalisation of a pipes cross-section occurs as it is exposed to a bending load which ultimately lead to the finding of a maximum bending moment. This non-linear response has been taken into account by the use of the *Nlgeom* function in ABAQUS. The simulation is run using a static general step with the Nlgeom option on.

To simulate accurate buckling behaviour to be observed, the automatic stabilization option in ABAQUS is used. A specific damping factor is employed to trigger the stabilization of the nonlinear quasi-static procedure. Viscous forces utilizing the damping factor are added to the global non-linear equilibrium equations (Ashraf, Morozov & Shankar, 2012). Selection of this damping factor was done by repetition of the simulation. Firstly, the Nlgeom option was turned off, and the model simulated linear behaviour of the pipe. Following this, the Nlgeom option was turned on, however no damping factor was specified. This simulated the non-linear behaviour of the pipe, with no buckling occurring. Finally, in order to select the appropriate damping factor, the simulation was run changing the damping factor each time. The ideal damping factor caused the response of the moment-rotation curve to correlate with both the linear and non-linear response. This correlation was achieved by using a damping factor of $c = 1\times10^{-08}$. As it can be seen in Figure 8, response of the simulation using a damping factor of $c = 1\times10^{-08}$ does correlate with the linear and non-linear responses.

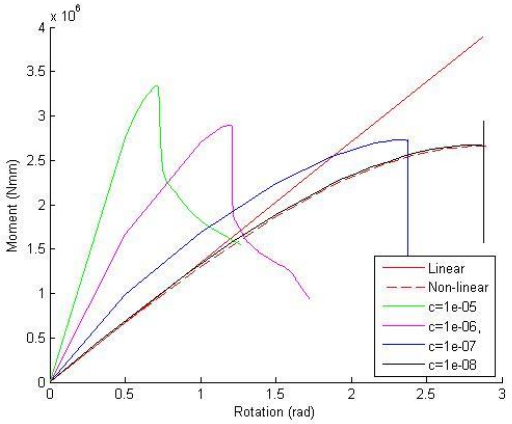


**Figure 8: Moment-rotation responses for different damping factors**

Validating the behaviour of the selected model for use in predicting the behaviour as a fully isotropic material pipe was undertaken. This was achieved by creating a composite layup consisting only of an isotropic material. As stated previously, the selected material was PE 80. The validation of this model was in calculating the critical moment at which buckling occurs. This was achieved by comparing the theoretical critical moment calculated by equation 11 (Kedward, 1978), and comparing this with the critical moment obtained via ABAQUS.

$$M_{cr} = \frac{2\sqrt{2}}{9}\frac{E\pi Rt^2}{\sqrt{1-\nu^2}} \tag{11}$$

The critical moment obtained via ABAQUS was achieved by producing a History Output of the Reaction Moment and Rotation at the reference point which the applied rotation displacement was applied. Furthermore, for a 50mm radius pipe, with wall thickness of 3mm and material properties of PE 80, the calculated $M_{cr}$ is 466550 Nmm and the corresponding value from ABAQUS is 456170 Nmm. It can be seen, the theoretical and obtained critical moments are within 2.5% of each other.

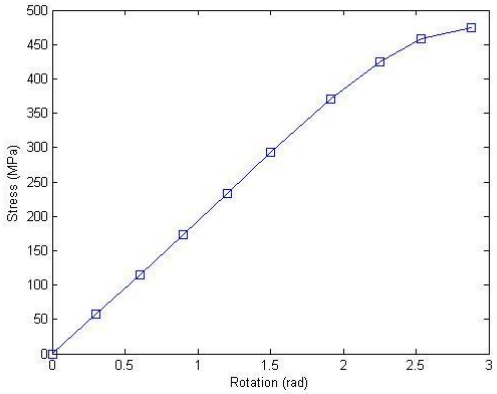


**Figure 9: Stress in the fibre direction due to applied rotation**

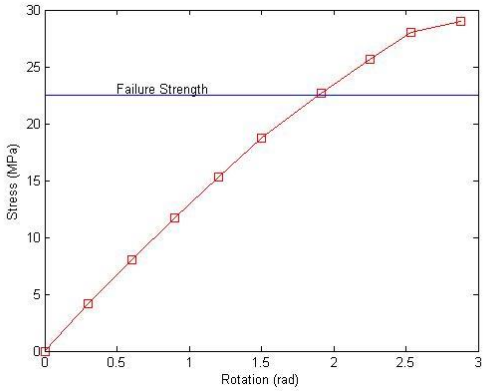


**Figure 10: Stress in the transverse direction due to applied rotation**

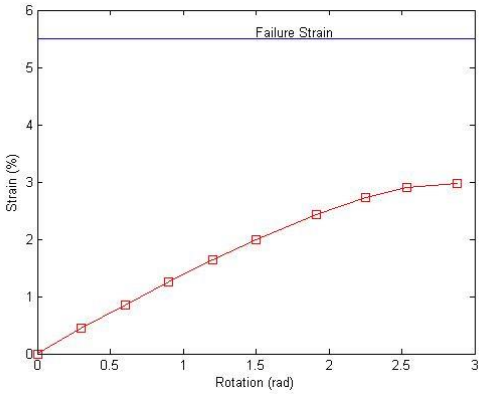


**Figure 11: Strain in the transverse direction due to applied rotation**

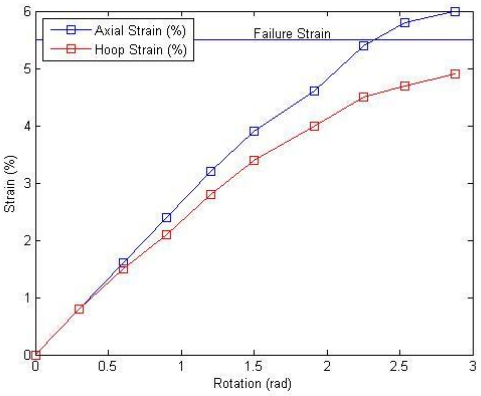


**Figure 12: Strains in the liner due to applied rotation**

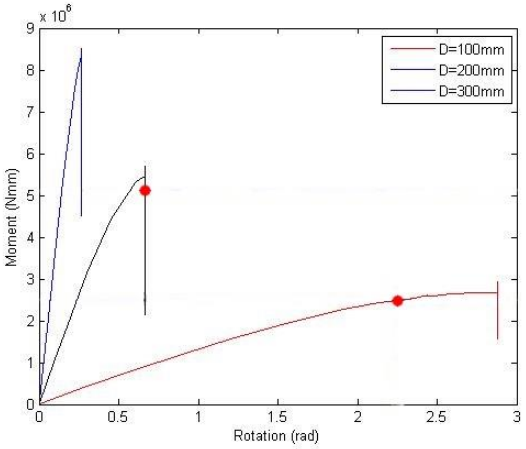


**Figure 13: Moment-rotation curves for three sizes of RTP**

Similarly, the same process was undertaken for a laminated pipe consisting of four Twaron fibre reinforced PE 80 plies. Using the same radius, and a wall thickness of 1.2mm the critical moment was calculated using equation 12 (Kedward, 1978), and was compared with the result obtained via ABAQUS.

$$M_{cr} = \frac{2\sqrt{2}}{9}\frac{E_x \pi R t^2}{\sqrt{1-\nu_x \nu_y}}\sqrt{\frac{E_y}{E_x}} \qquad (12)$$

where $E_x = \frac{A_{11}A_{22} - A_{12}^2}{A_{22}t}$ , $E_y = \frac{A_{11}A_{22} - A_{12}^2}{A_{11}t}$,

$\nu_x = \frac{A_{12}}{A_{22}}$ and $\nu_y = \frac{A_{12}}{A_{22}}$ (Tatting, 1998)

The theoretical critical moment obtained by equation 12, is equal to 339340 Nmm and the obtained critical moment from ABAQUS is 317531 Nmm. It can be seen that the theoretical and obtained values are within 6.5% of each other.

Therefore, based on the validation of the model for Isotropic and Laminated pipe models, the results obtained via ABAQUS for a full composite model can be assumed to be correct. This is because the full composite pipe is a combination of the Isotropic and Laminated pipe structures.

Consider a model that is 2m in length, has a lay-up previously discussed and a radius of 50mm, the results obtained from this buckling analysis can be seen in the following Figures.

It can be seen in the following Figures the stresses and strains induced in the pipe due to the applied rotation. Figure 9 shows that over the course of the applied rotation the stress in the fibre direction of the first ply is well below the material strength. Figure 10 shows the stress in the transverse direction, and it is showing that at 1.9125 rad (109.6°) if the material was brittle, the material would fail. However as it can be seen in Figure 11,

the strain in the transverse direction is well below the failure strain. Referring back to Figure 2, when the PE 80 reaches the 22.5 MPa limit, the stress ceases to increase and instead the strain increases. It can be seen in Figure 12 that material failure occurs in the liner at 2.25 rad (128.9°). Furthermore, in Figure 8, it can be seen using the damping factor of $c = 1\times10^{-08}$ , that buckling of the pipe occurs at 2.82 rad (161.6°). What this means is that material failure of the pipe is happening prior to buckling failure striking.

The same simulation was undertaken for two other pipe models, the only difference was that the pipe radiuses were 100 and 150mm respectively. The same analysis was undertaken to find out when failure took place. These results can be seen in Figure 13. For the pipe with a 200mm diameter, material failure occurred after buckling failure had transpired and for the pipe with a 300mm diameter, failure due to buckling happened well before material failure took place.

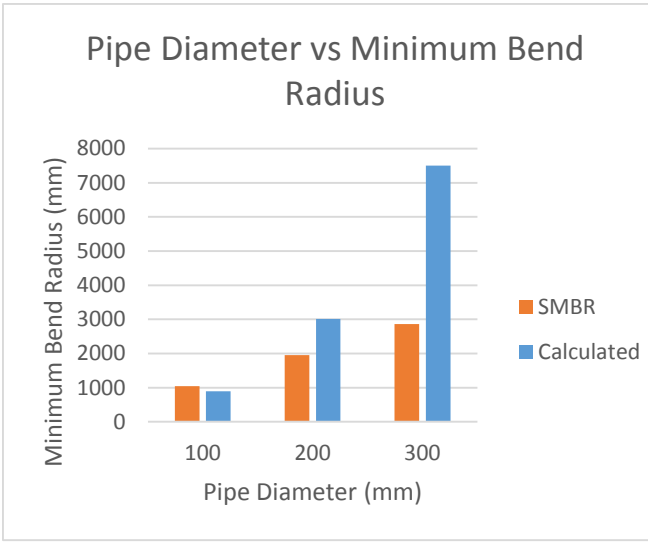


**Figure 14: Comparison of Minimum bend radius'**

As a result of the analysis' undertaken, it is possible to find the minimum bend radius of the pipe. This is done by taking the length of the pipe and dividing it by the critical rotation; the rotation at which failure occurs. This has been compared to the industry standard way of determining the storage minimum bend radius (SMBR) of the pipes found using, (Chapman et al, 2010)

$$SMBR = \frac{D_{outer}}{2\varepsilon_{fail}} \tag{13}$$

Where the outer diameter of the pipe is divided by the two times the failure strain of 5.5% as specified previously. It can be seen in Figure 14 the comparison between the SMBR and the calculated minimum bend radius' based on the analyses undertaken. As it can be seen, for the pipe of diameter 100mm, its minimum radius is in fact below the calculated SMBR. Comparatively, the calculated minimum radius obtained for the other two sized pipe is well over the SMBR.

This extremely large difference could potentially be attributed to the fact that pipes of these size have been found to buckle under a small rotational displacement.

This quickened buckling effect could be attributed to the fact that the ovalisation of the pipe is occurring much sooner, as the cross-section deforms much quicker in the larger pipe than to the smaller pipe. Furthermore, in calculating the SMBR, it is considering the material failure as the only mode of failure, when it can be seen in Figure 13 that for the 200mm and 300mm pipes that failure due to buckling does in fact occur prior to material failure.

## III. Conclusions

Modelling of the burst capacity and Spoolability of RTP has been undertaken. This is firstly to predict the burst capacity of various sized RTP and secondly to identify the mode of failure of various sized RTP when exposed to a bending load. The analysis into predicting the burst capacity of the RTP found that for smaller diameter RTP, there is a higher burst capacity of the pipe.

The analysis into the Spoolability of the RTP found that smaller sized pipes can be wound onto smaller sized reels. Furthermore the relationship between the empirical storage minimum bend radius calculation and the simulated results identified the need for failure due to buckling to be considered, as was the case with the larger sized RTP, the SMBR and calculated results were extremely different.

## IV. Recommendations

Further investigation into the non-linearity of the PE 80 should be conducted, primarily to identify if it plays any significant part in the scenarios analysed in this report. Additionally, the inclusion of thermal loadings due to internal pressure could be included to further predict the burst capacity of the RTP.

Potential investigation into the post-buckling behaviour of the RTP could be undertaken; primarily for those pipes where material failure occurs well after buckling. This would aid in understanding the behaviour of the pipes and identifying the critical point in which the pipe must be replaced.

## Acknowledgements

The author would like to thank the help of the academic staff at the University of New South Wales – Canberra for their assistance in completing the research. Furthermore, the efforts of Prof. Evgeny Morozov and Mr. Kuang Yu have been greatly appreciated in the conduct of the research.

## References

AMERICAN PETROLEUM INSTITUTE Recommended Practice 15S - Qualification of Spoolable Reinforced Plastic Line Pipe - FIRST EDITION

ASHRAF, M. A., MOROZOV, E. V. & SHANKAR, K. Flexure analysis of composite pipes during reeling process. Proceedings: the 7th Australasian Congress on Applied Mechanics (ACAM 7), 9-12 December 2012, the University of Adelaide, North Terrace Campus/National Committee on Applied Mechanics of Engineers Australia, 2012. Engineers Australia, 250.

BAI, Q. & BAI, Y. 2014. Subsea Pipeline Design, Analysis, and Installation, Gulf Professional Publishing.

BAI, Y., XU, F., CHENG, P., BADARUDDIN, M. F. & ASHRI, M. Burst Capacity of Reinforced Thermoplastic Pipe (RTP) Under Internal Pressure. ASME 2011 30th International Conference on Ocean, Offshore and Arctic Engineering, 2011. American Society of Mechanical Engineers, 281-288.

BRAZIER, L. 1927. On the flexure of thin cylindrical shells and other" thin" sections. *Proceedings of the Royal Society of London. Series A,* 116**,** 104-114.

CHAPMAN B, TUOHY J, BULMER G, BOLAM G, KALMAN M, SHELDRAKE T, SOENS C. Pipe and coupling design methodology for reinforced thermoplastic pipe (RTP) products. In: Proceedings of the 3rd composite materials for offshore operations. Houston; October 31–November 2 2010. p. 231–46.

CONLEY, J., WELLER, B. & SLINGERLAND, E. The Use of Reinforced Thermoplastic Pipe in Oil and Gas Gathering and Produced Water Pipelines. CIPC/SPE Gas Technology Symposium 2008 Joint Conference, 2008. Society of Petroleum Engineers.

DALMOLEN LGP, K. M., CLOOS PJ. Offshore application of "Reinforced Thermoplastic Pipe" (RTP) 4th Asian Conference & Exhibition, 2009 Kuala Lumpur, Malaysia.

HYDROCARBONS PRODUCTS SOLUFORCE. 2014. *Hydrocarbons:Products:SOLUFORCE: High Pressure Plastic pipe systems* [ONLINE] Available http://www.soluforce.net/products/hydrocarbons.php

KEDWARD KT. Nonlinear collapse of thin-walled composite cylinders under flexural loading. In: Proceedings of the 2nd international conference on composite materials (ICCM/2). Toronto; 1978. p. 353–65.

KRUIJER, M., WARNET, L. & AKKERMAN, R. 2005. Analysis of the mechanical properties of a reinforced thermoplastic pipe (RTP). *Composites Part A: Applied Science and Manufacturing,* 36**,** 291-300.

OSBORNE, J. 2013. Thermoplastic pipes–lighter, more flexible solutions for oil and gas extraction. *Reinforced Plastics,* 57**,** 33-38.

SHULTZ, M. & SMITH, L. V. Optimal fibre orientation for fibre reinforced pressure vessels. Proceedings of the SEM X International Congress & Exposition on Experimental & Applied Mechanics, Costa Mesa, California, USA, June, 2004. 7-10.

SULAIMAN, S., BORAZJANI, S. & TANG, S. Finite element analysis of filament-wound composite pressure vessel under internal pressure. IOP Conference Series: Materials Science and Engineering, 2013. IOP Publishing, 012061.

TATTING, B. F. 1998. *Analysis and design of variable stiffness composite cylinders.* Virginia Polytechnic Institute and State

TEIJIN ARAMID REINFORCED PIPES 2014. *Teijin Aramid Reinforced pipes* [ONLINE] Available http://www.teijinaramid.com/applications/reinforced-thermoplastic-pipes/

VASILIEV, V. V. & MOROZOV, E. 2013. *Advanced Mechanics of Composite Materials and Structural Elements*, Newnes.

YU, K., MOROZOV, E., ASHRAF, M. & SHANKAR, K. 2014. Analysis of flexural behaviour of reinforced thermoplastic pipes considering material nonlinearity. *Composite Structures*.